



Stable anatase TiO₂ formed by calcination of rice like titania nanorod at 800 oC exhibits high photocatalytic activity

Journal:	<i>RSC Advances</i>
Manuscript ID:	RA-ART-03-2014-001850.R2
Article Type:	Paper
Date Submitted by the Author:	02-May-2014
Complete List of Authors:	Grover, Inderpreet; Thapar University, School of Chemistry and Biochemistry Singh, Satnam; Thapar University, School of Chemistry and Biochemistry Pal, Bonamali; Thapar University, School of Chemistry and Biochemistry

ARTICLE

Stable anatase TiO₂ formed by calcination of rice like titania nanorod at 800 °C exhibits high photocatalytic activity

Cite this: DOI: 10.1039/x0xx00000x

Received 00th January 2012,
Accepted 00th January 2012

DOI: 10.1039/x0xx00000x

www.rsc.org/

Inderpreet Singh Grover^a, Satnam Singh^a and Bonamali Pal^a

This paper demonstrates the complete retention (> 98%) of anatase TiO₂ crystal phase at high temperature (800 °C) thermal treatment of rice like TiO₂ nanorods (length = 81-134 nm, diameter = 8-13 nm) relative to 100% conversion of rutile phase after calcination of P25-TiO₂ under similar condition. The existence of such anatase phase at > 800 °C was further confirmed by the presence of characteristic vibrational bands (144, 395, 513 and 639 cm⁻¹) in the Raman spectra. It was found that TiO₂ nanorods undergo fragmentation to highly crystalline irregular morphology (60-70 nm), nanopolygons (91-110 nm) and smaller rod shaped particles (length = 60-110 nm and diameter = 7-12 nm) accompanying gradual increase in their crystallite size (16 → 40 nm) and decrease in surface area (79-31 m²g⁻¹) with increased calcination temperatures from 200 to 900 °C. This TiO₂ anatase phase displayed enhanced photocatalytic oxidation rate (~2-11 times higher than rutile TiO₂) for methyl parathion (a neurotoxic pesticide) degradation to various intermediate products and ultimately to CO₂, where 1.0 wt% Au-TiO₂ significantly improved the photoactivity.

Introduction

Anatase TiO₂(TiO₂(A)) crystals because of its better surface properties, adsorptive affinity and greater rate of hole trapping efficiency is well proven (1-8) to exhibit improve photocatalytic activity than well known TiO₂ rutile (TiO₂(R)) phase. Also because of relative dissimilarity between the geometry of TiO₂(A) (tetragonal) and TiO₂(R) (distorted tetragonal) that originates from different arrangement of [TiO₆]²⁻ octahedral units, TiO₂(A) is reported to deliver higher photocatalytic activity (1,2,8) than TiO₂(R) because of indirect band gap character and presence of more hydroxylated groups on its surface. Whereas, TiO₂(R) phase shows its importance in case of P25-TiO₂ powder, a mixture of 80% anatase and 20% rutile, where it acts as an electron sink, hence showed superior photocatalytic activity (1,2,9) than its respective pure phase alone. The use of P25-TiO₂ for self cleaning agent in building materials requires high temperature (7,10) treatment during preparation of ceramic materials and for proper adherence to TiO₂ (mixed/coated) surface. This causes TiO₂(A)-to-TiO₂(R) phase transformation with a notable decrease in photocatalytic activity because of the formation of less photoactive TiO₂(R) phase (1-10) at > 600-700 °C. Therefore, highly crystalline

TiO₂(A) is needed without deteriorating photoactivity at high temperature, since high crystallinity led to fewer surface defects (7-10) acting as recombination sites for charge carriers, that consequently enhanced the photocatalytic activity.

Hence, various attempts (11-17) were made to resist TiO₂(A)-to-TiO₂(R) conversion at > 600 °C, and was achieved through surface modification with metal oxides (Al₂O₃, NiO, ZnO etc.) that renders this phase transformation. But the formation of secondary impurity phases (like Al₂TiO₅, NiTiO₃ etc.) resulted in decrease of photoactivity (16,17) and remained a major concern of this technique. Although, many reports (1,2) exist for the preparation of pure anatase TiO₂ at ambient conditions through a variety of routes, yet it showed moderate activity because of its poor crystallinity and amorphous nature. Hence, for the best efficiency, pure and stable TiO₂(A) phase at higher temperature (> 600 °C) without reducing the photocatalytic activity is highly desirable. The present study reveals that as-prepared TiO₂ nanorods are found to retain anatase crystal phase (~100%) by calcination at elevated temperatures (800-900°C) and displayed ~11 times better photocatalytic activity than conventional P25-TiO₂ calcined at the same temperature for photooxidation of methyl parathion (MP), a neurotoxic pesticide used (18,19) widely in agricultural fields. Moreover, the effect of Au deposition on the complete

decomposition of MP by this crystalline TiO₂(A) phase during UV-light irradiation is being discussed in-terms of CO₂ evolution and intermediate photoproducts formation by GC-MS analysis.

Materials

Sodium hydroxide (AR), Acetonitrile (HPLC), Methanol (GC), Ethyl acetate (GC), Isopropyl alcohol (AR) and Nitric acid were purchased from Loba Chemie. Commercially available P25-TiO₂ and MP were obtained from Degussa Corporation, Germany and Ravi Organics Pvt. Ltd. (Mumbai), India, respectively. Standard CO₂ gas (180 ppm) with N₂ as a base was obtained from Centurion Scientific Pvt. Ltd, New Delhi, India. All the chemicals were utilized without further purification.

Synthesis, characterization and photoactivity of TiO₂ nanocrystals

Synthesis of rice like anatase TiO₂ nanorods was carried through the hydrothermal route as reported (20) elsewhere. In a typical preparation, 4.73 g of P25-TiO₂ (P25) was mixed with 72 ml of 10 N NaOH and subjected to hydrothermal treatment at 130 °C in Teflon lined autoclave (80 ml capacity) for 20 h. The slurry was washed repeatedly with 0.1 N HNO₃, water and methanol. Aqueous slurry of thus obtained particles (3.2 g in 64 ml) at pH 5.6 (adjusted by 0.1 N HNO₃) was autoclaved at 175 °C for 48 h. The resulted slurry was filtered, washed with distilled water and methanol repeatedly, and dried at 70 °C in a hot air oven (Navyug Q-5267) for 3 h. These nanorod particles were calcined at 200-900 °C under aerial conditions in alumina crucibles using muffle furnace (Jupiter Scientific) for 2 h @ 3°C min⁻¹ rise of temperature and obtained samples are termed as C-2 to C-9 (calcined at 200-900 °C), respectively. The P25 was also calcined at 800 °C under similar conditions and abbreviated as P25(R). The photodeposition of Au (1 wt%) onto C-8 and P25 was carried (18) out in a test tube using de-aerated aqueous 5 ml (50%) isopropyl alcohol, 50 mg powder and required amount of AuCl₄.xH₂O under UV light (125 W Hg arc lamp) irradiation for 2 h. The Au³⁺ ions present in TiO₂ slurry are reduced to Au⁰ by the photoexcited electrons of TiO₂ and metal nanodeposits are formed throughout the TiO₂ surface which were washed with water and methanol, dried at 70 °C and used for the photocatalytic reactions. The Au-loaded samples thus obtained are abbreviated as Au-C-8 and Au-P25.

These samples were characterized through XRD (Panalytical X²-pert using Cu K α , λ =1.54178 Å), HR-TEM (Hitachi 7500, 2Å, 120 KV) for size-shape analysis. The BET surface area was measured with (Smart Sorb 93) using 150 mg of sample, preheated at 150 °C for 1 h, using calibration gases (N₂:He::70:30) at cryogenic temperature. Raman spectra (Renishaw system 2000 spectrometer) was obtained (100 to 800 cm⁻¹) using He-Ne laser operating at 514.5 nm. The photocatalytic activity of different titania catalysts was carried in a rubber capped test tube containing 5.0 mg of catalysts and 5 ml (50 ppm) aqueous solution of MP under UV light (125 W

Hg arc, 10.4 mW cm⁻²) irradiation for various time intervals. The reaction solution was analyzed by UV-visible spectrophotometer (Analytic-Jena Spectrod 205) and is calibrated (Electronic Supplementary Information (ESI)-fig.S1) with different concentration of MP. The quantitative estimation of CO₂ formed during its photooxidation was performed (17) on Gas Chromatograph (GC, NUCON-5765) equipped with Thermal Conductivity Detector (TCD). The gaseous sample (1 ml) was taken from the reaction vessel (gas tight test tube) and injected into Porapak-Q column having nitrogen as carrier gas (@30 ml/min). Column oven was maintained at 40 °C while injector and detector were kept at 70 and 80 °C, respectively.

GC (45X-GC)-Mass Spectrometer (MS-Scion-45P) analysis of MP photooxidation intermediates was carried out by collecting 3 ml reaction solution after 180 min of UV exposure in presence of Au-C-8 catalyst, followed by filtration (cellulose filter 0.22 μ m), extraction (with ethyl acetate, 3 \times 3 ml) and evaporated to dryness over rota-evaporator (Hedloph). Residue was dissolved in ethyl acetate (1 ml) and injected (1 μ l) to HP-5MS column (15m \times 0.25 mm \times 0.25 μ m) with flow rate of 1ml/min of Helium gas. The oven was programmed from 60 °C to 300 °C @ 6 °C/min rise of temperature. The injector and transfer line were isothermally kept at 250 °C and 275 °C, respectively.

Results and discussion

The XRD analysis (Fig. 1a) of the samples (C-2 to C-9) clearly showed the existence of TiO₂(A) as a major phase as revealed by its characteristic peaks (ICSD Card No.: 00-002-0387).

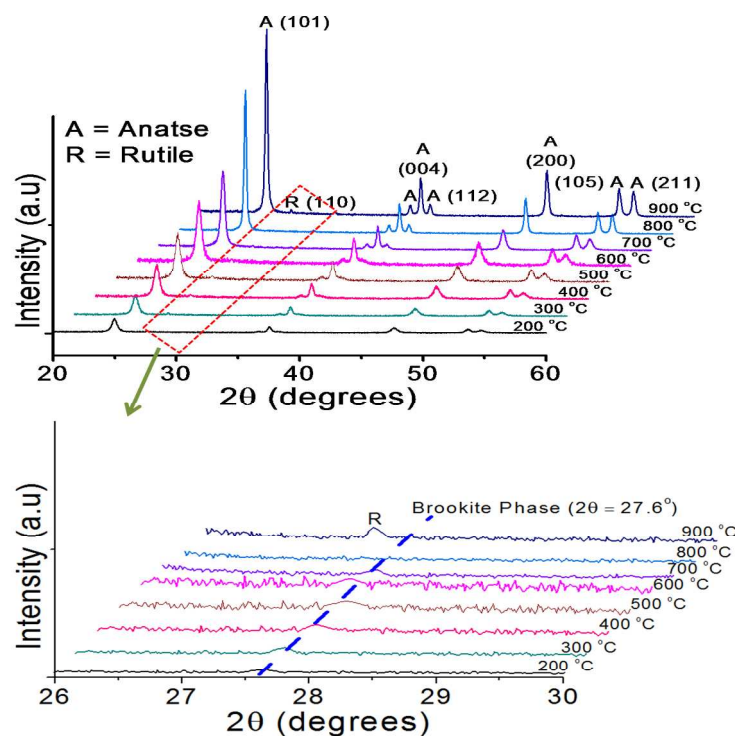


Fig. 1 XRD pattern for anatase TiO₂ (a) calcined at different temperatures and (b) their magnified view.

S. No	Catalyst	Weight Fraction of various crystal phases (%)			Average anatase crystallite size (nm)	Surface Area (m ² g ⁻¹)	Rate constant per unit surface area (k' × 10 ⁻¹) (min ⁻¹ m ⁻² g)
		Anatase	Brookite	Rutile			
1	P25(R)	--	--	100	--	55	0.013
2	P25					68	0.040
3	C-2	98.2	1.8	--	16	79	0.016
4	C-3	99.7	1.3	--	20	68	0.029
5	C-4	99.2	0.8	--	23	61	0.049
6	C-5	99.4	0.6	--	28	57	0.075
7	C-6	99.6	0.4	--	31	49	0.104
8	C-7	99.8	0.2	--	34	40	0.157
9	C-8	100	--	--	38	35	0.205
10	C-9	99.1	--	0.9	40	31	0.283

However, with gradual increase in calcination temperature (200-900 °C), there is a noticeable increase in intensity, sharpness and decrease in broadness for (101) peak at $2\theta = 25.3^\circ$ of TiO₂(A). In contrast, calcination of P25 at 800 °C resulted in complete transformation of its TiO₂(A) to TiO₂(R) phase as evidenced (ESI-fig.S2) through its characteristic (110) peak at $2\theta = 27.5^\circ$ (ICDS: Card No.: 00-001-1292). It is also seen that (Fig. 1b), some small peaks (at $2\theta = 27.6^\circ$) for brookite phase (ICDS: Card No.: 00-002-0514) were also present in C-2 to C-7 samples, while a new small peak for (110) plane of TiO₂(R) appears for C-9 sample. The co-existence of small amount of brookite phase (1.8-0.18 %) ca. as per reported method (1) with TiO₂(A) (Table 1) could be the cause (7,21) for its thermal stability, as the presence of brookite phase (21) obtained by the hydrolysis of tetrabutyl titanate in presence of surfactants imparted the thermal stability (> 700 °C) to TiO₂(A). The mean crystalline sizes of TiO₂(A) calculated using Scherrer equation (1) increases in the range 16-40 nm with increase in calcination temperatures from 200-900 °C (Table 1), indicating its gradual crystal growth (1,2,23) during thermal treatment. This is in well conformity with a recent report of Kang et al. (10), showing TiO₂(A) having crystallite > 14 nm retained (> 96%) even after calcination at 900 °C. However, some reports (24,25) also indicated TiO₂(A) size < 14 nm to be thermodynamically more stable than TiO₂(R) and resist towards conventional anatase-to-rutile transformation.

This crystal phase transformation was further confirmed by Raman spectra of four samples (C-2, C-5, C-8 and C-9; Fig. 2a-d). Three less intense and broad peaks at 247, 318 and 366 cm⁻¹

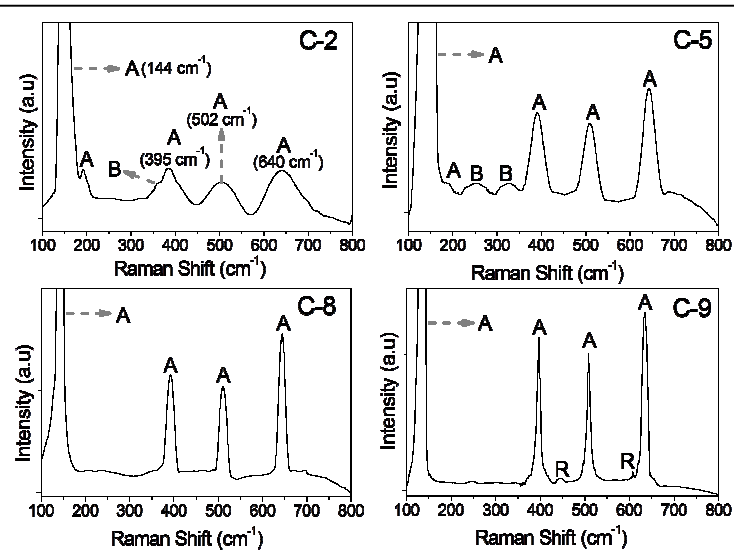


Fig. 2 Raman spectra of various calcined TiO₂ samples where A = Anatase, B = Brookite and R = Rutile phase.

for C-2 and C-5 (Fig 2a-b) samples corresponding (21) to A1g, B1g and B2g Raman vibration modes due to formation of small amount (1.8 - 0.18%, Table 1) of brookite phase. However, sample C-8 (Fig 2c) displayed only four intense and sharp peaks for Raman active vibration modes at 144, 395, 513 and 639 cm⁻¹ characteristics to TiO₂(A) (10,21). Interestingly, two very small peaks at 447 and 610 cm⁻¹ for C-9 catalyst due to growth of negligible amount (0.9%) of rutile phase (10) are observed along with four intense peaks (namely at 144, 395, 513 and 639 cm⁻¹) for TiO₂(A) as seen in Fig. 2d. This clearly confirms the retention (26) of crystalline anatase phase of TiO₂ at > 800 °C and is in agreement with XRD study.

Morphological study of C-2 (Fig. 3a), reveals rice like nanorods corresponding to length (L) = 81-134 nm and diameter (D) = 8-13 nm, obtained as per recent report of our group (20). With gradual increment in calcination temperatures from 200 to 500 °C and at 800 °C, fragmentation causes alteration in morphology from nanorods to a mixture of irregular shaped particles (~60-70 nm), few distorted rod-like shapes (L = 60-110 nm and D = 7-12 nm) (Fig. 3 b-c) and nanopolygons of size ~95-115 nm, (Fig. 3 e-f), respectively.

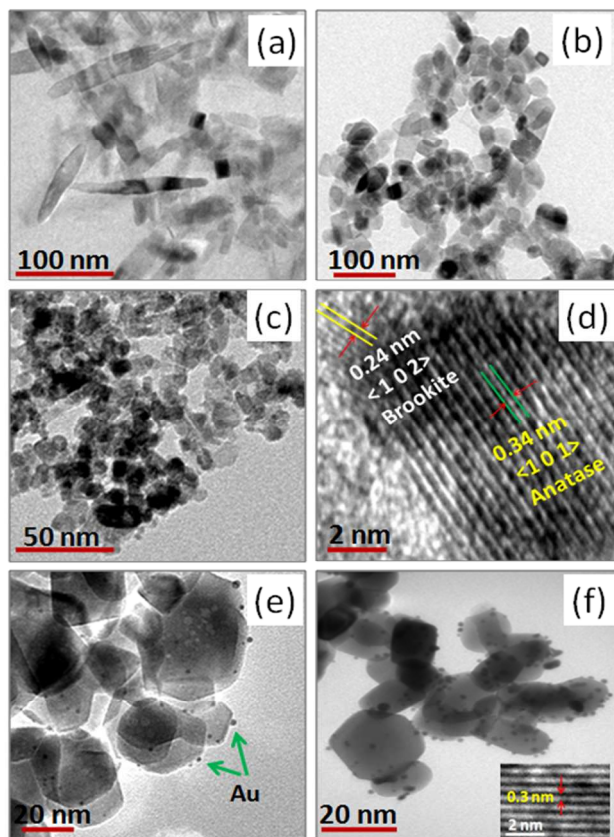


Fig. 3 HR-TEM images for calcined TiO₂ samples (a) C-2, (b and c) C-5, (d) lattice fringes of C-5 and (e and f) Au-C-8 with its lattice fringe (inset).

Although, there is no significant change in the morphology of P25 and P25(R), yet there is an increase in size from ~30-50 nm to ~70-80 nm, respectively (ESI-fig.S3). Due to the thermal fragmentation of C-5 and C-8 samples, few new particles with fresh and smooth surfaces, possessing fewer surface defects having more surface exposed atoms are formed that may show (1,2) better photocatalytic performance. This shape transformation is accompanied by decrease (Table 1) in specific surface area (S_{BET}) from 79 m²g⁻¹ to 57 m²g⁻¹ and then to 31 m²g⁻¹ for C-2, C-5 and C-8 samples, respectively. The increased particle size and decreased S_{BET} , accredited to their crystal growth during calcinations is in good agreement with the reported (1,2,23) results. The presence of characteristic lattice fringes 0.24 nm and 0.34 nm corresponding to brookite and

TiO₂(A) phase (Fig. 2d) confirms the existence of both crystal phases in C-5 catalyst. Whereas, for C-8, characteristic lattice fringe 0.3 nm belonging to TiO₂(A) (1,2,7,20) indicates the formation of pure anatase phase shown by XRD and Raman spectral studies. The TEM images of Au-C-8 (Fig. 3 e-f) showed many Au deposited TiO₂ nanoparticles having uniform deposition of Au nanoparticles (with narrow size distribution of 4-6 nm) over its surface. During the preparation of such stable and pure anatase TiO₂, no surfactant or other chemical reagent (except NaOH and HNO₃) was added that could hamper the photocatalytic activity (16,17), hence the present technique could be useful for optimizing the best photoactivity in many applications. The plots of $(\alpha h\nu)^{1/2}$ vs band gap energy (E_g) for TiO₂ (indirect semiconductor) in Fig. 4 revealed that E_g for P25 (3.1 eV) and C-2 (3.21 eV) are consistent with the reported values (1,20) and upon its calcination at 900 °C, E_g was reduced by 0.16 eV. As the particle and crystallite size of the as-prepared samples are found to increase gradually with the rise in calcination temperatures, therefore decrease in E_g values (1,20,21) is probably due to quantum size effect.

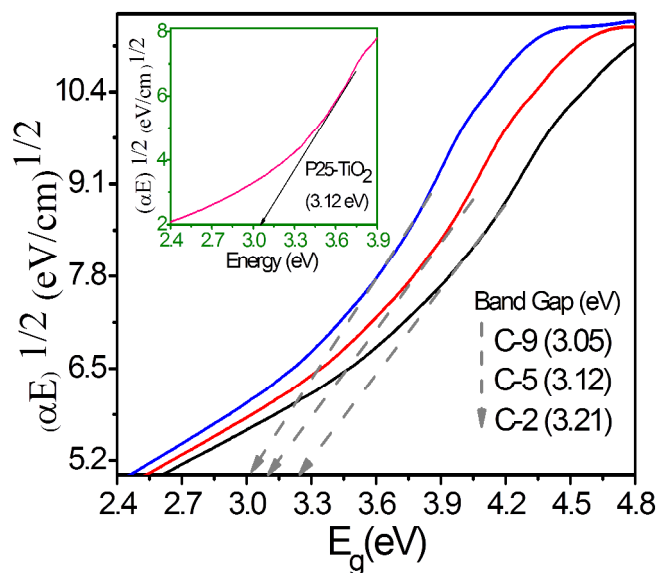


Fig. 4: Band gap energy of various TiO₂ samples as compared to (inset) P25-TiO₂ catalyst.

The time course of photocatalytic oxidation for MP by various titania catalysts calcined at different temperatures relative to bare P25 and P25(R) is shown in Fig. 5a. It can be seen that anatase-rutile mixed phases of P25 exhibited higher activity (inset Fig. 5b) than rutile TiO₂ (showing least activity among the studied photocatalysts) and 1 wt% Au loading onto P25 and C-8 catalysts further improved the MP degradation. The photooxidation of MP follows a linear relationship with irradiation time and decayed exponentially with increased calcination temperatures of C-2 to C-9 indicating (ESI-fig.S4) pseudo-first order kinetics. The apparent rate constants (k) obtained from time course graph gradually increased from 1.3×10⁻¹ min⁻¹ for C-2 to 8.8×10⁻¹ min⁻¹ for C-9 and becomes

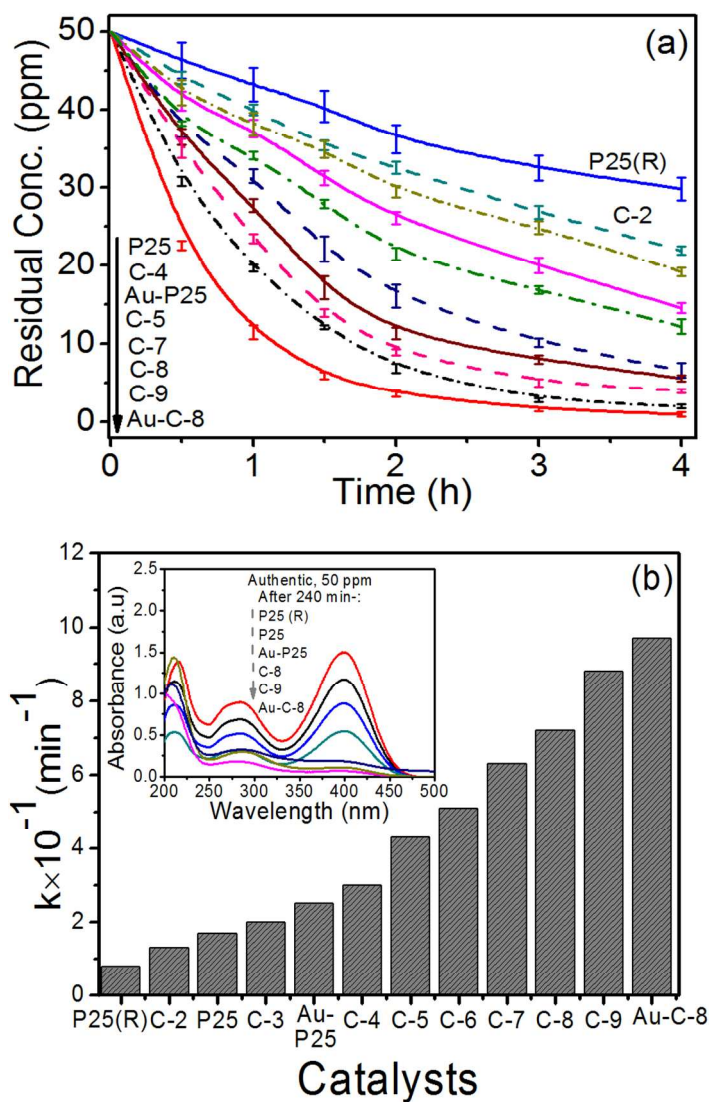


Fig. 5 (a) Time course of methyl parathion photooxidation by different calcined and 1wt% Au-deposited TiO₂ catalysts, and (b) their apparent rate constants; *inset*: absorption spectra for photooxidation of methyl parathion).

highest ($9.7 \times 10^{-1} \text{ min}^{-1}$) for Au-C-8 catalyst. Whereas, MP degradation efficiency exhibited by P25 ($k = 2.6 \times 10^{-1} \text{ min}^{-1}$) is highly reduced for P25(R) ($k = 0.78 \times 10^{-1} \text{ min}^{-1}$), revealing higher (2-11 times) photocatalytic activity of C-2 to C-9 catalysts as compared to the most active P25 catalyst.

After 120 min of UV irradiation, Au-C-8 catalyst although displayed complete degradation of MP ($47.1 \pm 0.4 \text{ ppm}$), yet incomplete mineralization occurs because of the formation of many smaller intermediate photoproducts as revealed by GC-MS analysis (Fig. 6), showing the formation of 4-hydroxynitrobenzene ($m/z = 140$), 4-methoxynitrobenzene ($m/z = 139$) and O,O,O-trimethyl thiophosphate ($m/z = 155$) intermediates. This indicates that longer irradiation time is needed to further decompose these intermediate products into

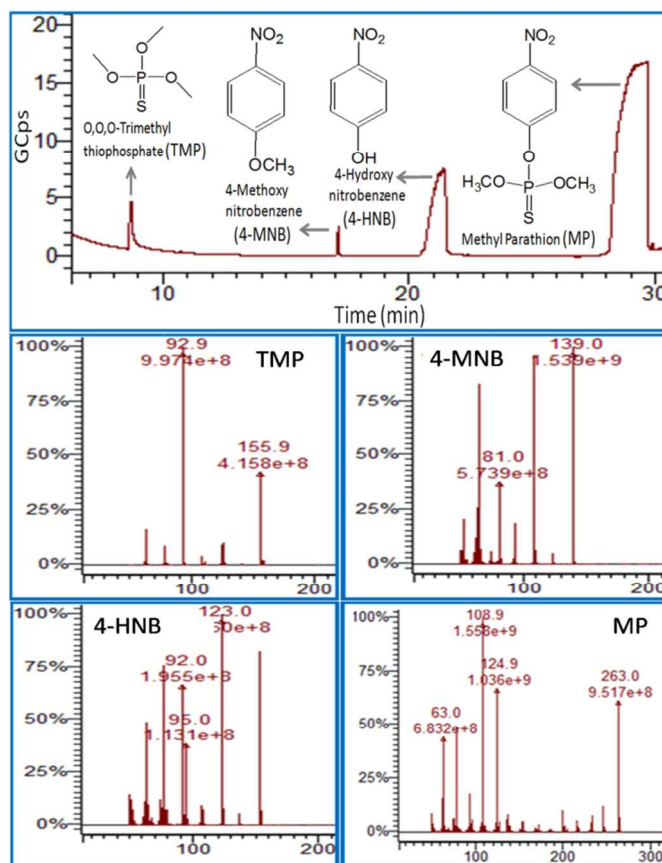


Fig. 6 GC-MS pattern of various intermediate photoproducts formed during methyl parathion degradation; *inset*: name and structural formula.

smaller molecules so that it can be completely mineralized to CO₂ and H₂O.

Time course of CO₂ formation (Fig. 7) during photooxidation of MP (ESI-fig. S5) by various titania catalysts showed a steady increase in CO₂ concentration with light irradiation. It was noticed that trends of CO₂ formation exhibited by different catalysts are similar to the MP photooxidation (Fig. 5), where superior catalytic activity of the calcined titania (C-3 to C-9) samples was observed than bare P25 and P25(R) catalysts. The highest amount (178 ppm) of CO₂ formed corresponds (ESI-table 1) to ~25 % by Au-C-8 catalyst followed by C-9 catalyst (156.2 ppm) indicating 22 % mineralization of MP during 4 h UV irradiation.

The presence of crystalline TiO₂(A) phases in calcined catalysts is believed to be the cause for their higher photocatalytic activity (1-10) as compared to pure rutile TiO₂ where existence of dominantly (110) plane are reported to act as a better reduction sites than oxidation sites (5). It was reported by Yu et al. (26) that increase in crystallinity of TiO₂(A) by calcining > 100 °C causes its enhanced photocatalytic activity than P25. The presence of interfacial contact between crystalline TiO₂(A) and brookite phases in C-2 to C-9 is expected to facilitate the migration (21,27) of photoexcited holes from anatase to the brookite phase due to

higher valance band edge of former (3.1 eV vs NHE) than later (3.0 eV vs NHE) resulting in their higher efficiency for MP oxidation. While in case of P25, transfer of only electrons from $\text{TiO}_2(\text{A})$ to $\text{TiO}_2(\text{R})$ phase occurs, resulting in less suppression of charge recombination process than anatase-brookite TiO_2 interface (21), hence showing lower photoactivity than the as-prepared calcined titania samples.

The detrimental influence (1,2,16,20,24) of increased crystallite size (16-40 nm) and decreased surface area ($79\text{-}31\text{ m}^2\text{g}^{-1}$) for the photocatalytic activity of calcined catalysts was not observed. As a result, the enhanced photoactivity of C-2 to C-9 catalysts can be ascribed to the increasing crystallinity that generally reduce the defect sites for relaxation of photoproducted electron-hole pairs (1,2,11-17) for $\text{TiO}_2(\text{A})$.

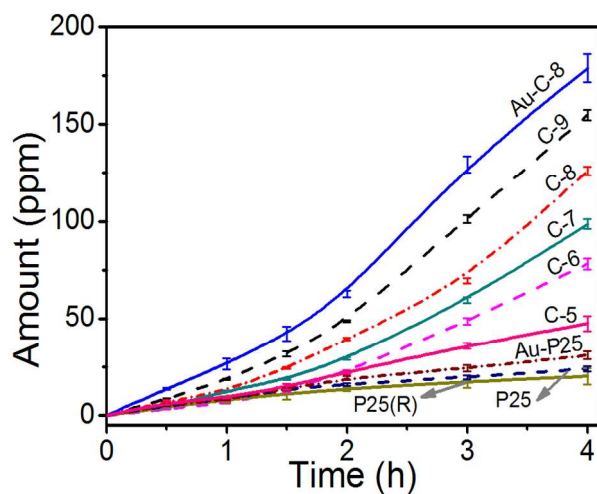


Fig. 7 CO_2 formation rate during photooxidation of methyl parathion by different TiO_2 catalysts.

This photoactivity could also be correlated by the rate constant per unit surface area (k_1) in Table 1, where $k_1 = 0.283 \times 10^{-1} \text{ min}^{-1}/\text{m}^2\text{g}^{-1}$ for C-9 is higher than $k_1 = 0.016 \times 10^{-1} \text{ min}^{-1}/\text{m}^2\text{g}^{-1}$ for C-2, $k_1 = 0.04 \times 10^{-1} \text{ min}^{-1}/\text{m}^2\text{g}^{-1}$ for P25 and $k_1 = 0.013 \times 10^{-1} \text{ min}^{-1}/\text{m}^2\text{g}^{-1}$ for P25(R) catalysts. Thus, despite of decreasing surface area with increased calcination temperatures, the photoactivity per unit surface area is increased relative to P25 catalyst. Therefore, it can be emphasized that improvement in crystallinity (7) diminishes the recombination of excited charge carriers resulting in enhanced photoactivity.

Moreover, there is notable and significant increase in intensity of (101) planes with increasing calcination temperatures, thus causing more (101) surface facets serving as adsorption sites of electron scavenging O_2 molecules facilitating the formation of more oxidative superoxide radicals (9) and is responsible for the highest activity of C-9 catalyst. The Au-loading notably improves the photocatalytic activity owing to the rapid charge transfer and Fermi energy level equilibrium at the Au- TiO_2 interface, suppresses (1,2,23,28) the charge recombination process and thereby enhances the photocatalytic activity.

Conclusion:

In summary, it is concluded that rice like anatase TiO_2 In summary, it is concluded that rice like anatase TiO_2 nanorods retains its anatase crystal structure after calcination at $> 800^\circ\text{C}$, whereas P25- TiO_2 catalyst is converted to rutile phase under similar experimental conditions. Although, increase in crystallinity and rate constant per unit surface area of this as-prepared stable anatase TiO_2 crystal phase played a vital role for superior photoactivity for MP degradation, yet the detrimental influences of decreased surface area, and increased particle and crystallite size are not observed for these C-2 to C-9 catalysts that are thermally treated at high temperatures.

Acknowledgements

The authors acknowledge the University Grants Commission and Department of Science and Technology, New Delhi, Government of India for providing financial support. Degussa Corporation, Germany) is gratefully acknowledged for the gift sample of TiO_2 .

Notes and references

^a School of Chemistry and Biochemistry, Thapar University, Patiala 147004, Punjab (India), *E-mail: bpal@thapar.edu, Tel: 91-175-2393128, Fax: 91-175-2364498

References

1. X. Chen and S. S. Mao, *Chem. Rev.*, 2007, **107**, 2891–2959.
2. A. Kudo and Y. Miseki, *Chem. Soc. Rev.*, 2009, **38**, 253–278.
3. J. Yan, G. Wu, N. Guan, L. Li, Z. Lib and X. Cao, *Phys. Chem. Chem. Phys.*, 2013, **15**, 10978–10988.
4. J. C. Yu, J. Lin, D. Lo and S. K. Lam, *Langmuir*, 2000, **16**, 7304–7308.
5. N. Wu1, J. Wang, D. N. Tafen, H. Wang, J. G. Zheng, J. P. Lewis, X. Liu, S. S. Leonard and A. Manivannan, *J. Am. Chem. Soc.*, 2010, **132**, 6679–6685.
6. G. S. Herman, Z. Dohnalek, N. Ruzycycki and U. Diebold, *J. Phys. Chem. B*, 2003, **107**, 2788–2795.
7. W. Li, Y. Bai, C. Liu, Z. Yang, X. Feng, X. Lu, N. K. V. D. Laak, and K. Y. Chan, *Environ. Sci. Technol.*, 2009, **43**, 5423–5428.
8. T. Luttrell, S. Halpegamage, J. Tao, A. Kramer, E. Sutter and M. Batzill, *Scientific reports*, 2014, **4**, 4043–4050
9. D. C. Hurum, A. G. Agrios, K. A. Gray, T. Rajh and M. C. Thurnauer, *J. Phys. Chem. B*, 2003, **107**, 4545–4549.
10. C. Kang, L. Jing, T. Guo, H. Cui, J. Zhou and H. Fu, *J. Phys. Chem. C*, 2009, **113**, 1006–1013.
11. R. Arroyo, G. Cordoba, J. Padilla and V. H. Lara, *Mater. Lett.*, 2002, **54**, 397–402.
12. S. Sabale, A. Bandgar, H. Wang, K. Gurav, J. H. Kim and S. H. Pawar, *Met. Mater. Int.*, 2013, **19**, 483–488.
13. H. Zhang and J. F. Banfield, *J. Phys. Chem. B*, 2000, **104**, 3481–3487.

14. M. S. P. Francisco and V. R. Mastelaro, *Chem. Mater.* 2002, **14**, 2514–2518.
15. D. J. Reidy, J. D. Holmes, C. Nagle and M. A. Morris, *J. Mater. Chem.*, 2005, **15**, 3494–3500.
16. S. C. Pillai, P. Periyat, R. George, D. E. McCormack, M. K. Seery, H. Hayden, J. Colreavy, D. Corr and S. J. Hinder, *J. Phys. Chem. C*, 2007, **111**, 1605–1611.
17. C. Kang, L. Jing, T. Guo, H. Cui, J. Zhou and H. Fu, *J. Phys. Chem. C*, 2009, **113**, 1006–1013.
18. E. Moctezumaa, E. Leyvaa, G. Palestinoa and H. de-Lasa, *J. Photochem. Photobiol. A-Chem.*, 2007, **186**, 71–84.
19. I. K. Konstantinou, T. M. Sakellarides, V. A. Akkas, and T. A. Albanis, *Environ. Sci. Technol.*, 2001, **35**, 398–405.
20. I. S. Grover, S. Singh, B. Pal, *Appl. Surf. Sci.*, 2013, **280**, 366–372.
21. G. Tian, H. Fu, L. Jing, B. Xin, K. Pan, *J. Phys. Chem. C*, 2008, **112**, 3083–3089
22. Y. Hu, H. L. Tsai, C. L. Huang, *J. Eur. Ceram. Soc.*, 2003, **23**, 691–696.
23. I. S. Grover, S. Singh, B. Pal, *J. Nanosci. Nanotechnol.*, doi:10.1166/jnn.2014.9072.
24. A. S. Barnard and H. Xu, *ACS Nano*, 2008, **2**, 2237–2242.
25. H. Zhan and J. F. Banfield, *J. Mater. Chem.*, 1998, **8**, 2073–2076.
26. J. C. Yu, J. Yu, W. Ho, Z. Jiang, L. Zhang, *Chem. Mater.*, 2002, **14**, 3808–3816.
27. W. Li, C. Liu, Y. Zhou, Y. Bai, X. Feng, Z. Yang, L. Lu, X. Lu, K. Y. Chan, *J. Phys. Chem. C*, 2008, **112**, 20539–20545
28. X. Zhang, Y. L. Chen, R. S. Liu and D. P. Tsai, *Rep. Prog. Phys.*, 2013, **76**, 46401–46442.

Graphical Abstract:

